Journal of Loss Prevention in the Process Industries 83 (2023) 105016

Contents lists available at ScienceDirect

Journal of Loss Prevention in the Process Industries

journal homepage: www.elsevier.com/locate/jlp

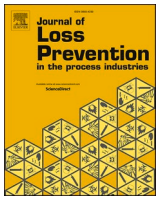

Dust particle sedimentation in the 20 L standard vessel for dust explosion tests

Maria Portarapillo [a,*], Roberto Sanchirico [b], Almerinda Di Benedetto [a]

[a] Department of Chemical, Materials & Production Engineering, University of Naples Federico II, Naples, Italy
[b] CNR, Institute of Sciences and Technologies for Sustainable Energy and Mobility (STEMS), Naples, Italy

ARTICLE INFO

Keywords:
Standard test vessels
Dust explosion
Dust sedimentation
Partial feeding

ABSTRACT

According to the current international standards, to perform the correct evaluation of the explosion and flammability parameters, a uniform distribution of the dust particles should be achieved inside the 20 L and/or 1 m^3 standard vessels.

CFD simulations have shown that in both standard test vessels (20 L and 1 m^3), the dust particles are not uniformly dispersed, being mostly concentrated at the edge of the macro-vortices generated by the injection of the fluid and particle through the nozzle. In addition, only a partial fed of the particles is obtained, and dust particles sedimentation phenomena can occur.

As a result, the dust participating to the reactive process may be much lower than the expected nominal concentration in the vessel due to sedimentation and incomplete feeding. Consequently, misleading values of the flammability/explosion parameters could be measured.

Particle sedimentation and incomplete feeding depends both on the Stokes number and on the Reynolds number, whereas the concentration distribution depends on the turbulence level, the fluid flow maps, and the number of particles which enter into the vessel through the nozzle.

The aim of this work is to evaluate the key parameters (particle size, particle density, and fluid velocity) affecting sedimentation and incomplete feeding in 20 L vessel. To this end, CFD simulations of dust dispersion are performed at varying the particle density and size. Operating maps, in terms of the key parameters and/or their dimensionless combinations, are developed and a correlation for correction of the data is proposed.

1. Introduction

To quantify the explosibility of combustible dusts, explosion testing is carried out in spherical closed vessels of 20 L and/or 1 m^3. Whatever the vessel used, the measured explosion parameters should be the same. However, several discrepancies were found among the results obtained in the two vessels although standard procedures were followed (ASTM E1226-19, 2019; BS EN, 2011, 2012).

Results strongly depend on several factors.

- Dust size (Bartknecht, 1989; Di Sarli et al., 2013; Portarapillo et al., 2021c; Shag and You, 2013);
- Dust shape (Di Sarli et al., 2019; Marmo and Cavallero, 2008; Portarapillo et al., 2022a);
- Chemical ignitors explosion (Cashdollar, 2000; Cashdollar and Chatrathi, 1992; Cloney et al., 2013; Clouthier et al., 2020; Di Benedetto et al., 2012; Gao et al., 2013; Going et al., 2000; Mintz, 1995; Portarapillo et al., 2021a; Rodgers and Ural, 2011; Taveau et al., 2017).

In addition, pre-ignition turbulence plays a major role in affecting the explosion behaviour. As a result, the control of the turbulence level in both vessels is of primary importance (Cashdollar, 1996; Di Benedetto et al., 2012). Over the years, some doubts arise about the generally accepted ignition delay time of 60 ms in the 20 L sphere which could be too short to create turbulent conditions equal to the larger standard vessel. For this reason, the small vessel was used to determine the role of turbulence in the dust flame propagation. Di Benedetto et al. (2012) performed measurements of the pressure history of methane/nicotinic acid/air mixtures in the 20 L Siwek sphere, by changing the ignition delay time (t_d), and then the pre-ignition turbulence. From the obtained results, the violence of the explosion of an hybrid mixture decreases as t_d

* Corresponding author.
E-mail address: maria.portarapillo@unina.it (M. Portarapillo).

https://doi.org/10.1016/j.jlp.2023.105016
Received 11 October 2022; Received in revised form 1 February 2023; Accepted 22 February 2023
Available online 25 February 2023

Table 1
Dust properties used for simulation.

Diameter (μm)	Density (kg/m^3)
10	500–7000
60	500–7000
100	500–7000
200	500–7000
400	500–7000

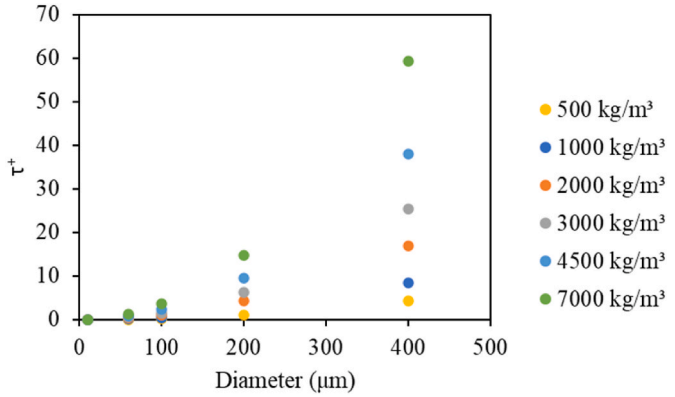

Fig. 1. Dimensionless relaxation time as a function of the diameter and parametric in the density.

increases independent of the ignition energy level (Di Benedetto et al., 2012). Several authors measured the turbulence level inside the 20 L sphere (Dahoe et al., 2002; Mercer et al., 2001; Pu et al., 1990; van der Wel et al., 1992) and the 1 m^3 spherical/cylindrical vessel (Hauert and Vogl, 1995; Zhen and Leuckel, 1996). Results showed that the turbulent conditions in the 20 L sphere at 60 ms were considerably more intense than the conditions in the large vessel at the (standard) ignition delay time (Pu et al., 1990).

Turbulence is required for dispersing dust particles at a fairly uniform concentration to ensure reliable and repeatable estimation of safety parameters (ASTM E1226-19, 2019; ASTM E1515-14, 1993; ASTM E2931-13, 2013; BS EN 14034-1, 2004; ISO 6184–1:1985, 1985). Some researchers investigated the effectiveness of dust dispersion in various test vessels using optical dust probes in the 20 L sphere (Kalejaiye, 2001; Kalejaiye et al., 2010) and in the 1 m^3 ISO vessel (Cashdollar and Chatrathi, 1992; Hauert and Vogl, 1995). Generally, the measurements are based on the attenuation by absorption and dispersion of a light beam penetrating the dust cloud. Kalejaiye et al. used optical dust probes to measure optical transmittance through the dust cloud at six locations within the 20 L sphere, with both the standard dispersion nozzles. They tested the dispersion of three different dusts and results showed that the transmission data of the three dusts were significantly lower than those corresponding to the nominal value. They attributed this difference to the reduction in particle size that occurred during dispersion (Kalejaiye, 2001; Kalejaiye et al., 2010). Cashdollar and Chatrathi (1992) carried out comparisons between the uniformity of the dust cloud formed in the 20 L chamber and Fike 1 m^3 test vessel, using optical dust probes. They observed that the 1 m^3 transmission data were somewhat lower than in the 20 L chamber at low dust concentrations. A possible explanation for this behaviour is an increased agglomeration in the 20 L chamber (Cashdollar and Chatrathi, 1992). Hauert and Vogl (1995) measured the dust concentration of maize starch (diameter 15 μm, density 1000 kg/m^3, nominal concentration 120 g/m^3) in the 1 m^3 vessel at 9 different locations. Results showed differences in the

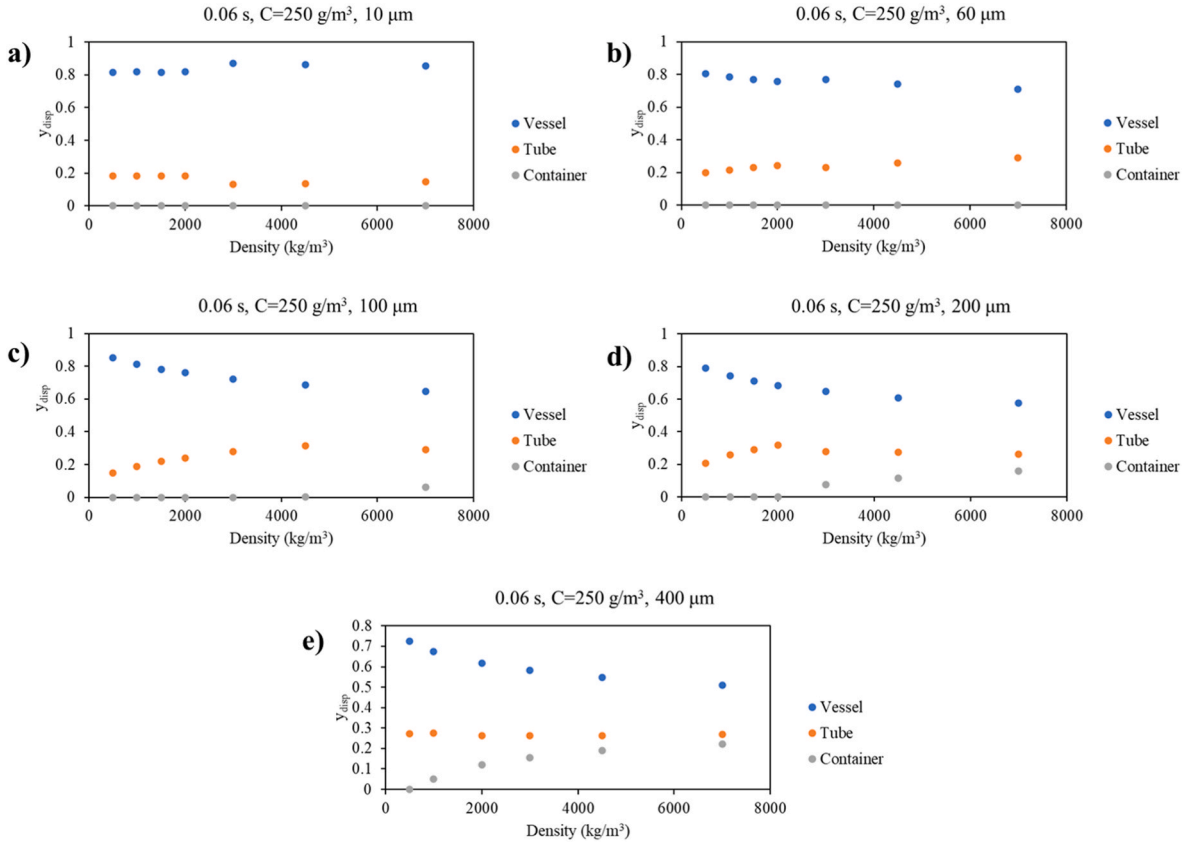

Fig. 2. Dispersed mass-to-nominal mass (y_{disp},C_{nom} = 250 g/m^3) ratio at 10 μm (a), 60 μm (b), 100 μm (c), 200 μm (d), 400 μm (e) as a function of density at the ignition delay time in the vessel (blue scatter plot), the tube (orange scatter plot) and the container (grey scatter plot). (For interpretation of the references to colour in this figure legend, the reader is referred to the Web version of this article.)

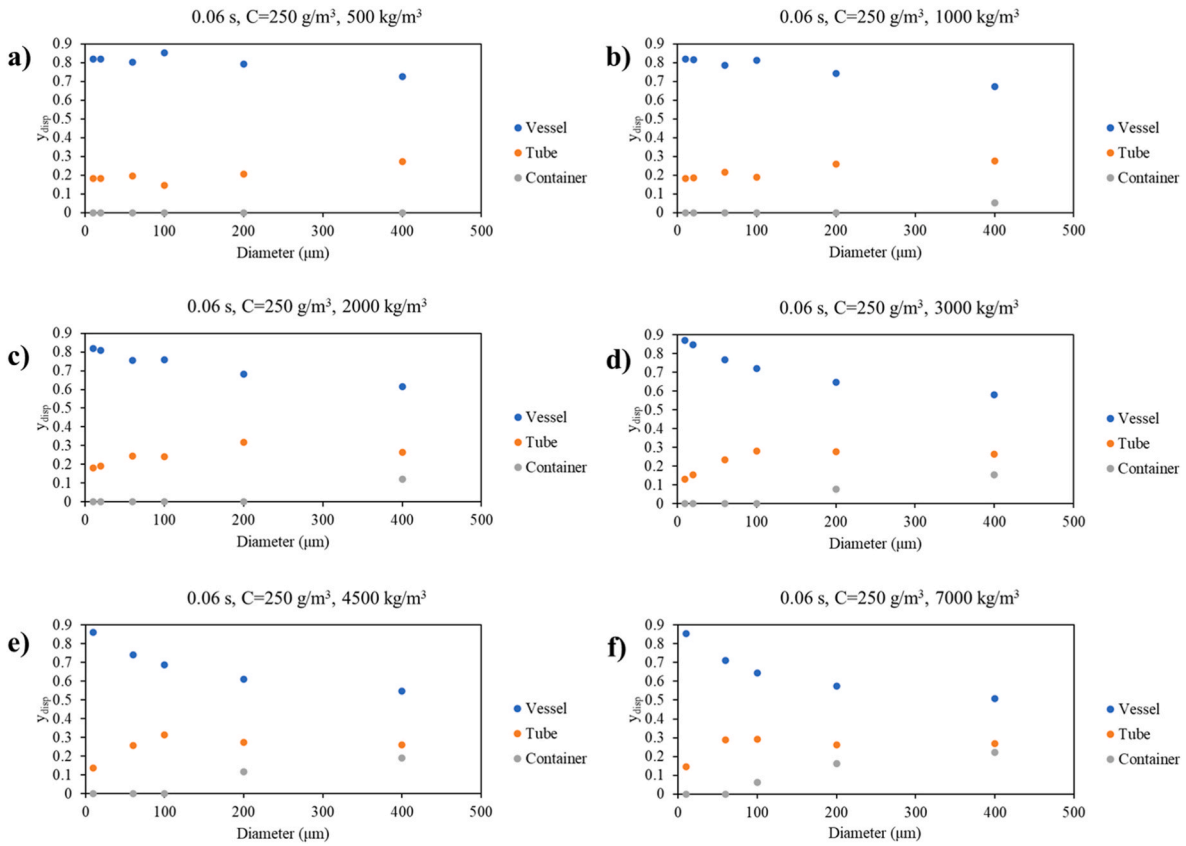

Fig. 3. Dispersed mass-to-nominal mass (y_{disp}, C_{nom} = 250 g/m^3) ratio at 500 kg/m^3 (a), 1000 kg/m^3 (b), 2000 kg/m^3 (c), 3000 kg/m^3 (d), 4500 kg/m^3 (e) and 7000 kg/m^3 (f) as a function of diameter at the ignition delay time in the vessel (blue scatter plot), the tube (orange scatter plot) and the container (grey scatter plot). (For interpretation of the references to colour in this figure legend, the reader is referred to the Web version of this article.)

transmission data at the different points, indicating that the dust cloud is non-uniform. In particular, the highest values of dust concentration were found on the bottom of the vessel due to sedimentation (Hauert and Vogl, 1995). These results were confirmed by CFD simulations carried out by our research group. The computed maps of turbulent kinetic energy show significant spatial variation of the turbulent kinetic energy in the 20 L vessel. Conversely, in the 1 m^3 vessel, the turbulence level is much more uniform (Di Benedetto et al., 2013; Portarapillo et al., 2022b; Portarapillo et al., 2020b). The different level of pre-ignition turbulence also introduces qualitative differences in terms of the turbulent combustion regime that is established following ignition. In particular, within the smaller vessel there will be greater interaction of the flame front with turbulent vortices while in the 1 m^3 the propagation is nearly laminar (Portarapillo et al., 2021b). As regard the dust concentration and distribution, the dust is mainly concentrated at the outer zones of the vortices generated in the vessels (whatever nozzle is used) and then dust concentration is not uniform (Di Benedetto et al., 2013; Portarapillo et al., 2022b; Portarapillo et al., 2020b).

In a previous work regarding the dispersion of mixtures of niacin and anthraquinone, we showed that due to the different properties (size and density) of the two pure dusts, there were some zones richer in niacin and poor in anthraquinone concentration and vice versa compromising the reliability of the test and the evaluation of any parameter relating to the mixture (Portarapillo et al., 2020a). We then concluded that the powder temporal/spatial dispersion strongly depends on the properties of the dust such as diameter and density. From all these results, we may conclude that the generation of a uniform cloud is then affected by the spatial/temporal fluid flow inside the vessel, by the efficiency of the feeding from the container to the vessel and by particle sedimentation.

In this work we investigate the role of diameter and density of dust particles on partial feeding and sedimentation. To this end we simulated the dust dispersion in the 20 L sphere at changing the dust size and density, eventually quantifying the impact of particle sedimentation and partial feeding on the dust concentration distribution.

2. Methodology

CFD simulations were carried out under the operating conditions contained in Table 1 with a nominal dust concentration set at 250 g/m^3. In this preliminary work, monodispersed dusts with diameter from 10 to 400 μm were considered. In the case of size distribution the conclusions achieved by this work can be extended since the system can be considered as dispersed (Elghobashi, 1994). The details of CFD simulations are reported in a previous work (Di Benedetto et al., 2013). The used equations are well reported in (Portarapillo et al., 2022b). Briefly, the model consists of the continuity and momentum conservation equations (Eulerian approach), solved by using the standard k-ε model as turbulent sub-model with standard wall function and considering compressibility effects. The fluid flow equations were discretized using a finite-volume formulation on the three-dimensional non-uniform unstructured grid (478,449 elements). The flow of the solid phase was solved with the Lagrangian formulation using the Discrete Phase Model (*DPM*). The used geometry was divided into three partitions: the vessel, where the explosion test occurs, the feeding tube, that connect the vessel to the dust container, and the container itself, where the dust is charged.

Theoretically, the effect of concentration should also be investigated. Indeed, the dust concentration does not seem to have a direct effect on the sedimentation phenomenon but indirectly affects it by modifying the flow field of the continuous phase. At this stage, the interest is focus on a low value of concentration (250 g/m^3) for two reasons: this value is the first tested during explosion screening and some dusts are characterized by a MEC value in the range of 200–250 g/m^3. It is worth underlining

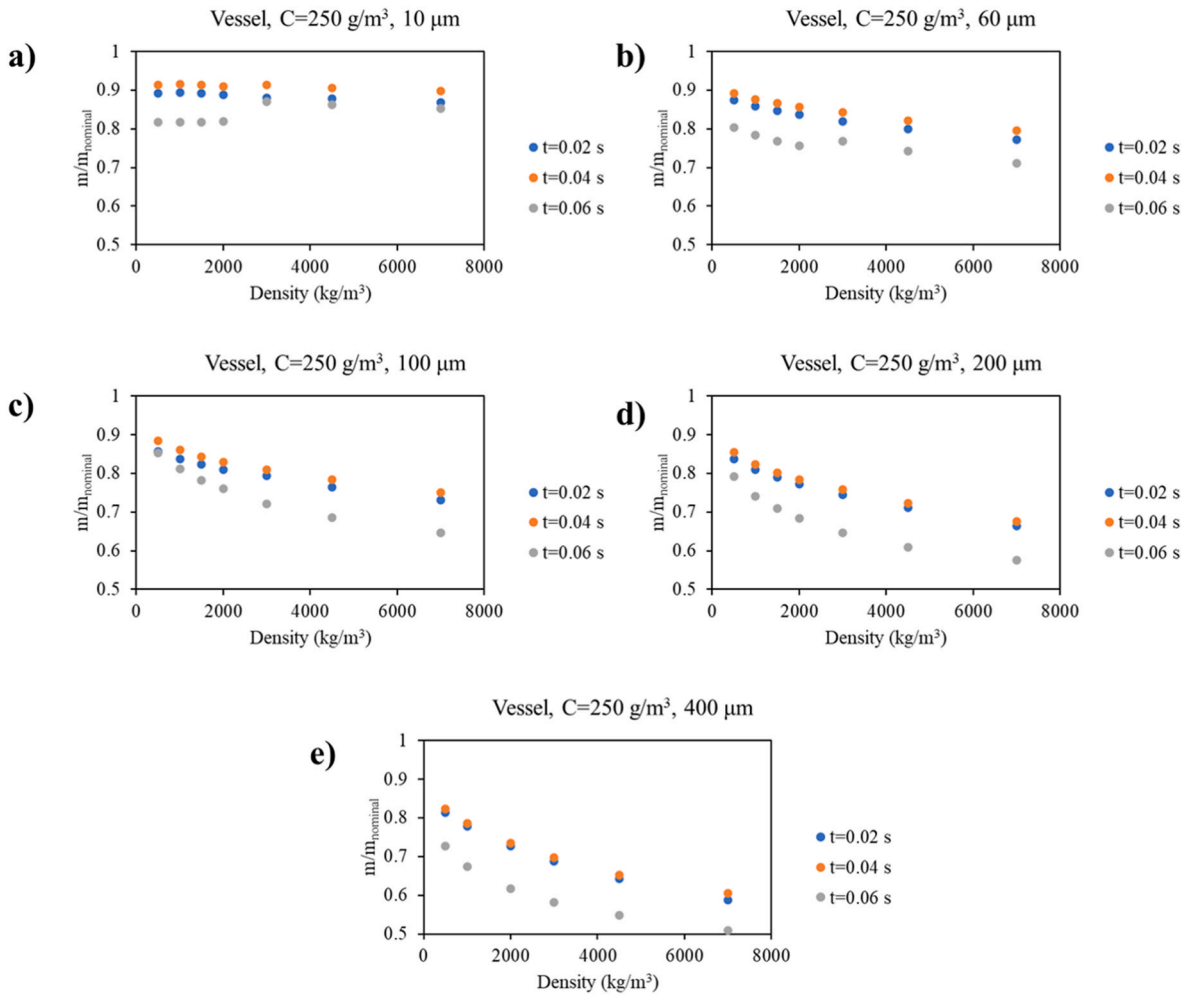

Fig. 4. Y_{disp} (C_{nom} = 250 g/m^3) in the explosion vessel at 10 µm (a), 60 µm (b), 100 µm (c), 200 µm (d), 400 µm (e) as a function of density within the explosion vessel at 0.02 s (blue scatter plot), 0.04 s (orange scatter plot) and 0.06 s (grey scatter plot). (For interpretation of the references to colour in this figure legend, the reader is referred to the Web version of this article.)

that the dust aliquot that remains dispersed in the form of a cloud inside the sphere is the one that, once triggered the explosion, contributes to it. The rest of the powder will form a layer on the base of the vessel and on the rebound nozzle. To this aim, the mass fractions of dispersed dust (y_{disp}) present in the different domain partitions (vessel, tube and container) at different instants of time (0.02,0.04,0.06 s) were calculated as a function of the dimensionless relaxation time τ^+. In particular, to consider if a particle sedimented or not, the particles where tracked in terms of position and velocity in each partition. The criterium used for sedimentation was position <10% of the domain size and velocity <0.01 m/s. Especially, from the results of the simulations through the filter (position <10% of the domain size and velocity <0.01 m/s) in each simulation, we determined the deposited mass and, using the volume integral, the total mass present in each partition. The difference was used to obtain the dispersed mass and thus the dispersed dust fraction in each partition.

Y_{disp} and τ^+ were defined as reported in Equation (1) and Equation (2):

$$y_{disp} = \frac{m_{disp}}{m_{tot}} = \frac{m_{disp}}{C_{nom} \cdot V} = 1 - y_{dep} \tag{1}$$

$$\tau^+ = \frac{\tau}{t_d} = \frac{\rho_p d_p^2}{18 \cdot \mu \cdot t_d} \tag{2}$$

where m_{disp} (kg) is the dispersed dust mass within the 20 L sphere, m_{tot} (kg) is the total dust mass fed in the 20 L sphere corresponding to the nominal concentration value, C_{nom} (kg/m^3) is the nominal dust concentration fed to the standard test vessel, V (m^3) is the vessel volume, τ (s) is the relaxation time, t_d (s) is the ignition delay time, ρ_p (kg/m^3) is the particles density, d_p (m) is the particles size, μ (Pa•s) is the air dynamic viscosity. As regards the deposited dust fraction (y_{dep}) this can be evaluated as complement to 1 of the dispersed dust fraction if the amount of trapped dust can be neglected.

The relaxation time is the characteristic time for the particle to approach steady motion. It characterizes the time required for a particle to adjust or "relax" its velocity to a new condition of forces and is an indication of the particle ability to quickly adjust to a new environment or condition. Since relaxation time is proportional to the square of particle diameter, it increases rapidly with the increase of particle size. Usually, small particles "relax" to new environments (i.e., following the flow well) in a very short time, while larger particles are more "stubborn" and tend to stick to their original path.

3. Results and discussion

In Fig. 1, the dimensionless relaxation time is shown as a function of the dust diameter, at different values of the dust density. The dimensionless value increases both with dust diameter and density.

Fig. 2 shows the dispersed mass-to-nominal mass ratio (y_{disp}) present within the vessel, the tube, and the container at the ignition delay time,

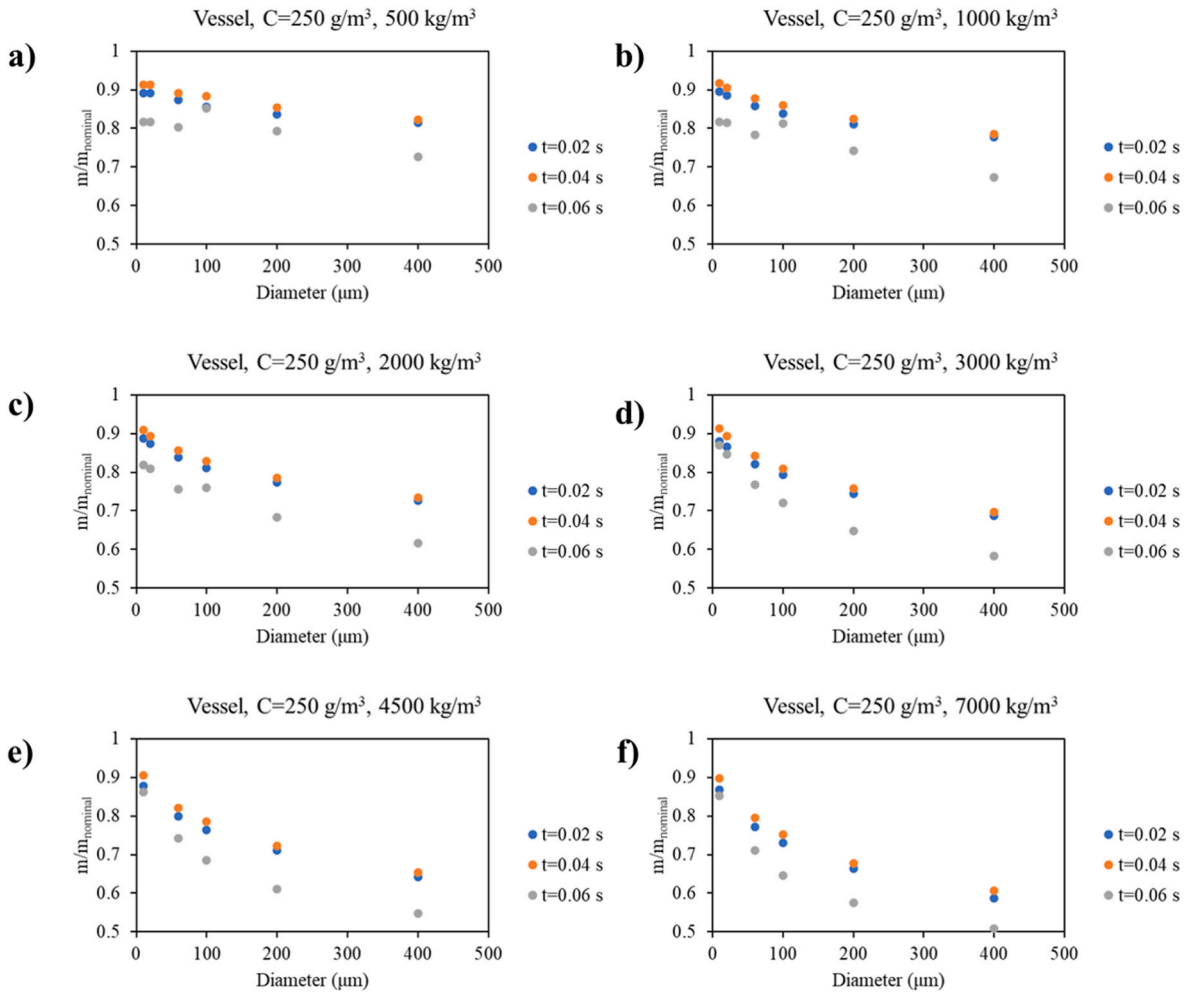

Fig. 5. Y_{disp} (C_{nom} = 250 g/m^3) in the explosion vessel at 500 kg/m^3 (a), 1000 kg/m^3 (b), 2000 kg/m^3 (c), 3000 kg/m^3 (d), 4500 kg/m^3 (e) and 7000 kg/m^3 (f) as a function of diameter within the explosion vessel at 0.02 s (blue scatter plot), 0.04 s (orange scatter plot) and 0.06 s (grey scatter plot). (For interpretation of the references to colour in this figure legend, the reader is referred to the Web version of this article.)

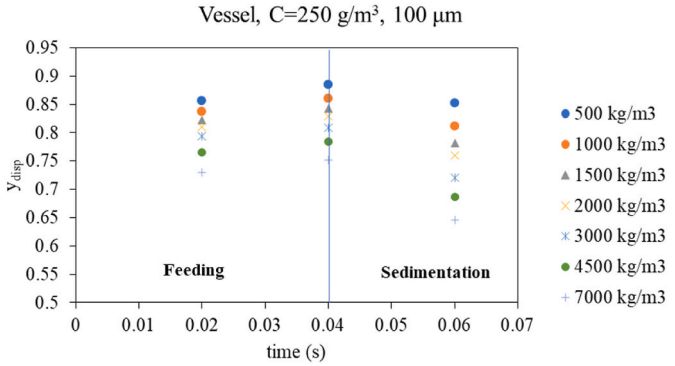

Fig. 6. Mass fraction of dispersed dust in the explosion vessel as a function of time and parametric in the density values, C_{nom} = 250 g/m^3, 100 μm.

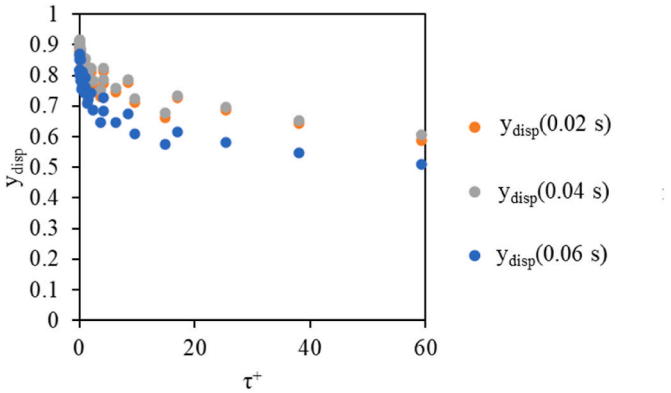

Fig. 7. Mass fraction of dispersed dust in the explosion vessel as a function of the dimensionless relaxation time and parametric in time.

as computed at different values of diameter and density. At low values of the dust diameter (<100 μm) the dispersed mass-to-nominal mass ratios within all the three parts of the whole domain are less sensitive to density variations. As the diameter increases, the dependence on the density is more relevant, the y_{disp} ratio decreases in the explosion vessel while it increases both in the tube and in the container. It is worth noting that in the case of the dust container, the fraction of dispersed dust is always low (<0.2 in the worst case), while there is always a large amount of dust in the feeding tube. The presence of dust in this section of the domain is a clear symptom of partial dust feeding, which must nevertheless be taken into account.

The same behaviour was found at low values of density (<1000 kg/m^3) where y_{disp} within all the three parts of the whole domain are less sensitive to diameter variations as the trends are almost horizontal (Fig. 3).

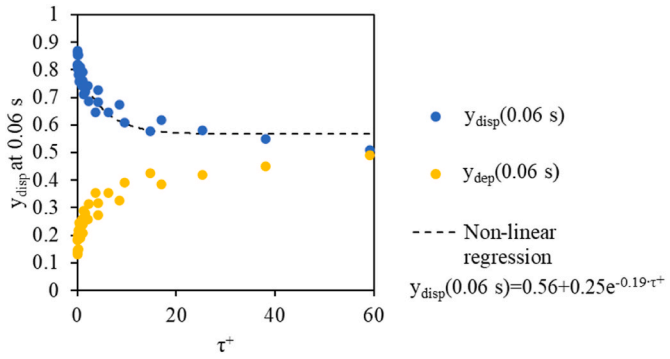

Fig. 8. Mass fraction of dispersed and deposited dust (including settled dust inside the explosion vessel and dust present inside the other domains) in the explosion vessel at 0.06 s as a function of the dimensionless relaxation time. A non-linear regression (3-factors exponential decay) for y_{disp} is also shown (R^2 = 0.91).

It is worth noting that in the case of low concentrations the fraction of dust remaining in the container after dispersion is practically negligible. This behaviour is also verified by the results shown in Fig. 2 (a, b, c) and Fig. 3 (a, b,c). From diameters of more than 200 μm and/or densities of more than 2000 kg/m^3, the fraction of dust remaining in the container begins to increase (with a maximum value of 20% of the total mass). This behaviour is therefore typical of particularly coarse and/or dense dust, such as metallic dust.

The trends of y_{disp} within the explosion vessel are shown as function of density at different values of the diameter (Fig. 4) and as function of the diameter at different values of the density (Fig. 5), parametric in time. It was found that y_{disp} significantly decreases as both density and diameter increase, starting from a maximum value equal to 0.86 and reaching a plateau value at 0.50.

Starting from the results reported in Figs. 4 and 5, two phases can be identified.

- feeding phase: the fraction of dust dispersed in the vessel increases from 0.02s to 0.04 s
- sedimentation phase: the fraction of dust dispersed in the vessel decreases from 0.04 s to 0.06 s

These phases are also shown by way of example for 100 μm dust in terms of the fraction of dust dispersed in the vessel as a function of time in Fig. 6.

To summarize all the results, Fig. 7 shows the fraction of dust dispersed (y_{disp}) inside the vessel versus the dimensionless relaxation time (τ^+), parametric in time. Notably, the fraction increases during the feeding phase (up to 0.04 s the pressure gradient still allows the dust to enter from the container and the tube within the 20 L vessel). After this phase, it decreases due to the sedimentation phenomenon.

All the data may be plotted as function of the relaxation time (τ^+), as shown in Figs. 7 and 8. It is found that the higher τ^+, the longer the time required for the fluid to involve the dust particles in the turbulent motion generated by the pressure gradient. If the dust is not involved in the swirling motion generated in the sphere, it will tend to settle on the bottom of the vessel and will not participate to the flame propagation. In the case of dusts characterized by high relaxation time values, the fraction dispersed at the ignition delay time is equal to 50% of the nominal value. This turns out to be very critical both for the evaluation of P_{max} and K_{St} (which would be underestimated) but above all in the evaluation of the *MEC* which could be largely overestimated. Fig. 8 also shows the non-linear regression of the data obtained for the fraction of dispersed dust y_{disp} in the vessel at the ignition delay time. The regression equation (**Equation (3)**) is as follows:

$$y_{disp}(0.06\ s, explosion\ vessel) = 0.56 + 0.25e^{-0.19\tau^+} \quad (3)$$

In Fig. 9 the data are combined in an operational map (density/diameter) and different zones are identified.

1) size-driven zone: density does not play any effect (blue zone, diameter <100 μm). Indeed, as shown and discussed in Fig. 2, at low values of the dust diameter (<100 μm), the fraction of dispersed dust within all the three parts of the whole domain are less sensitive to density variations. This means that, in this zone, given different dusts characterized by the same size, the fraction of dispersed dust inside the vessel at the ignition delay time is the same whatever the density value, as the correction of the nominal concentration.
2) density-driven zone: diameter does not play any effect (yellow zone, density <1000 kg/m^3). Indeed, as shown and discussed in Fig. 3, at low values of density (<1000 kg/m^3) where ydisp within all the three parts of the whole domain are less sensitive to diameter variations as the trends are almost horizontal. This means that, in this zone, given different dusts characterized by the same density value, the fraction of dispersed dust inside the vessel at the ignition delay time is the same whatever the size, as the correction of the nominal concentration.

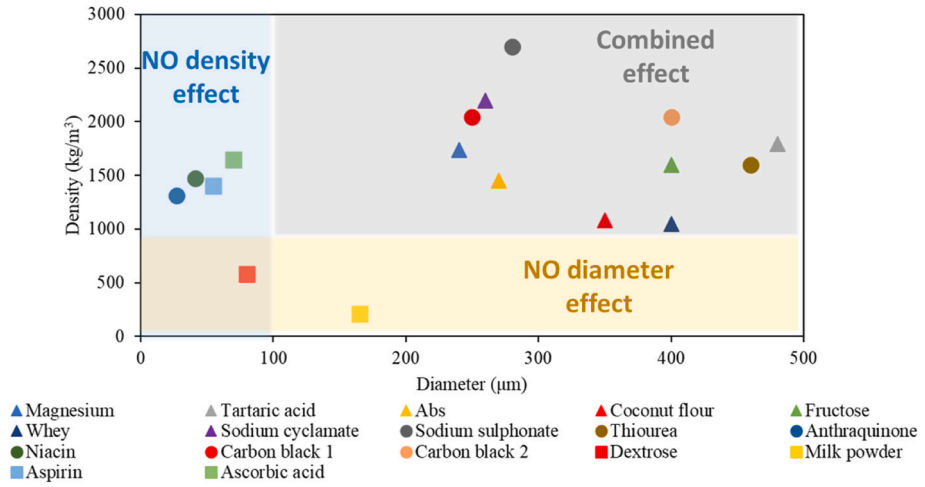

Fig. 9. Density-diameter plane with areas of influence of the parameters highlighted in different colours: no density effect (blue), no diameter effect (yellow) and combined effect (grey). Typical combustible dusts are also reported. (For interpretation of the references to colour in this figure legend, the reader is referred to the Web version of this article.)

3) combined zone: both diameter and density affect dust dispersion (grey zone). Indeed, for dust diameter higher than 100 μm and density higher than 1000 kg/m^3, the fraction of dispersed dust within all the three parts of the whole domain is sensitive to both density and diameter variations.

Some combustible dusts are reported in Fig. 9 to show that typically the dusts can fall into each of the areas described above. The operational map of Fig. 9, may be used to derive a procedure for the minimising the effect of sedimentation and partial feeding.

Following the procedure, before testing the dust, the operator should.

a) calculate the relaxation time (τ^+), knowing the dust size and density;
b) calculate the fraction of dust dispersed through the non-linear regression reported in **Equation (3)** to assess the maximum deviation of the nominal concentration and, if necessary, to proceed with a correction;
c) check from Fig. 9 if, in the case of non-monodispersed sample, changes in diameter due to fragmentation or formation of agglomerates and changes in density, the fraction of material needs to be modified.

In the following paragraph, an example of procedure application is reported.

Example.

a) Dust size: 50 μm

Dust density: 1500 kg/m.^{3}
Calculated dimensionless relaxation time τ^+: 0.19.

b) Calculated fraction of dispersed dust y_{disp}: 0.8

Correction needed? Yes, the concentration effectively tested is 20% lower than the nominal one. All the explosion parameters have to be intended valid for a reduced dust concentration.

c) Zone: size-driven zone

Correction needed? A correction of y_{disp} is mandatory in case of size variation of the dust (fragmentation, agglomeration etc.) but not in case of density modifications.

4. Discussion of hypothesis and results

In this work, several assumptions were made. In particular, the dust concentration was set to a constant value of 250 g/m^3, the dust particles are spherical and the particles are all monodisperse. Notably, the concentration of the powder, as well as the shape and diameter of the particles, have a strong influence on the velocity flow field within the container and thus on the dust dispersion itself at the ignition delay time. As reported in the Methodology section, this value was chosen since it is the first tested during explosion screening and some dusts are characterized by a MEC value in the range of 200–250 g/m^3.

As regard the effect of shape, this can be taken into account by using the equivalent diameter instead of the actual diameter when calculating the dust relaxation time. To account for the variation in diameter, if the particle size distribution of the sample is known, the application of the proposed method can be performed using the volume-weighted averaged diameter value and also perform evaluations for fine and coarse fractions.

It is worth noting that the proposed procedure may have an applicative impact on the safety parameters evaluation, in particular on the measurement of the minimum explosive concentration that is the one most affected by the sedimentation phenomenon. Particularly, the sedimentation can cause an overestimation of MEC due to a lower dust aliquot actually involved in the explosion. However, the dust sedimentation also plays a role in the evaluation of the maximum explosion pressure and the deflagrative index. Indeed, it is important to emphasise that the dust concentration modifies the turbulent flow field within the sphere and thus the dispersion of the dust itself. Thus, the effect of sedimentation is present, whatever the dust concentration value. Consequently, the presence of the dust and its sedimentation have an effect on the explosion pressure and the maximum rate of pressure rise at each concentration. Therefore, the maximum value used for the design of the safety measures can also be strongly influenced, and this becomes increasingly so as the relaxation time increases.

5. Conclusions

In this work, the effect of sedimentation and partial injection was quantified by CFD simulation of dust dispersion in a 20 L sphere. Several simulations were performed under change of diameter and density (and consequently under change of relaxation time). Due to sedimentation and partial feeding, a lower dust aliquot than the nominal value is tested and the results in terms of explosion parameters cannot be considered reliable. The results showed that at lower values of the diameter, the density has no influence on the proportion of dust dispersed in the vessel at the ignition delay time and that at low density, the diameter has no influence on the same variable.

To correct for the concentration present in the vessel during an explosion test and the explosion parameters obtained, a correction should be made. We have proposed a correlation between the proportion of dust actually involved in the explosion and the relaxation time of the dust.

Credit author statement

Maria Portarapillo: Methodology; Investigation; Conceptualization; Writing – original draft; Writing – review & editing, Roberto Sanchirico: Writing – review & editing, Almerinda Di Benedetto: Conceptualization; Writing – original draft; Writing – review & editing; Resources; Supervision.

Declaration of competing interest

The authors declare that they have no known competing financial interests or personal relationships that could have appeared to influence the work reported in this paper.

Data availability

No data was used for the research described in the article.

Acknowledgement

The authors warmly thank Eng. Luigi Di Giacomo for the modelling support during his Master's thesis.

References

ASTM E1226-19, 2019. Standard Test Method for Explosibility of Dust Clouds. ASTM Int. West Conshohocken, pp. 1–15. https://doi.org/10.1520/E1226-19. PA.
ASTM E1515-14, 1993. Standard Test Method for Minimum Explosible Concentration of Combustible Dusts 1. ASTM Int., pp 1–9. https://doi.org/10.1520/E1515-14. West Conshohocken, PA.
ASTM E2931-13, 2013. Standard Test Method for Limiting Oxygen (Oxidant) Concentration of Combustible. ASTM Int. West, Conshohocken, PA. https://doi.org/10.1520/E2931-13.
BS EN, 2011. Determination of Maximum Explosion Pressure and the Maximum Rate of Pressure Rise of Gases and Vapours, 15967, 2012.
Bartknecht, 1989. Dust Explosions.
BS EN 14034-1, 2004. Determination of Explosion Characteristics of Dust Clouds Part 1: Determination of Maximum Pressure Pmax of Dust Clouds 3.

Cashdollar, K.L., 1996. Coal dust explosibility. J. Loss Prev. Process. Ind. 9, 65–76. https://doi.org/10.1016/0950-4230(95)00050-X.
Cashdollar, K.L., 2000. Overview of dust explosibility characteristics. J. Loss Prev. Process. Ind. 13, 183–199. https://doi.org/10.1016/S0950-4230(99)00039-X.
Cashdollar, K.L., Chatrathi, K., 1992. Minimum explosible dust concentrations measured in 20-L and 1-M3 chambers. Combust. Sci. Technol. 87, 157–171. https://doi.org/10.1080/00102209208947213.
Cloney, C.T., Ripley, R.C., Amyotte, P.R., Khan, F.I., 2013. Quantifying the effect of strong ignition sources on particle preconditioning and distribution in the 20-L chamber. J. Loss Prev. Process. Ind. 26, 1574–1582. https://doi.org/10.1016/j.jlp.2013.08.010.
Clouthier, M.P., Ogungbemide, D., Cloney, C., Zalosh, R.G., Ripley, R.C., Amyotte, P.R., 2020. Numerical investigation of overdriving in the 20-L Siwek chamber. In: 13 Th International Symposium on Hazards, Prevention and Mitigation of Industrial Explosions ISHPMIE2020 Physikalisch-Technische Bundesanstalt, pp. 663–676. https://doi.org/10.7795/810.20200724.
Dahoe, A.E., Cant, R.S., Scarlett, B., 2002. On the decay of turbulence in the 20-liter explosion sphere. Flow, Turbul. Combust. 67, 159–184. https://doi.org/10.1023/A:1015099110942.
Di Benedetto, A., Garcia-Agreda, A., Russo, P., Sanchirico, R., 2012. Combined effect of ignition energy and initial turbulence on the explosion behavior of lean gas/dust-air mixtures. Ind. Eng. Chem. Res. 51, 7663–7670. https://doi.org/10.1021/ie201664a.
Di Benedetto, A., Russo, P., Sanchirico, R., Di Sarli, V., 2013. CFD simulations of turbulent fluid flow and dust dispersion in the 20 liter explosion vessel. AIChE 59, 2485–2496. https://doi.org/10.1002/aic.
Di Sarli, V., Russo, P., Sanchirico, R., Di Benedetto, A., 2013. CFD simulations of the effect of dust diameter on the dispersion in the 20L bomb. Chem. Eng. Trans. 31, 727–732.
Di Sarli, V., Danzi, E., Marmo, L., Sanchirico, R., Di Benedetto, A., 2019. CFD simulation of turbulent flow field, feeding and dispersion of non-spherical dust particles in the standard 20 L sphere. J. Loss Prev. Process. Ind. 62, 103983 https://doi.org/10.1016/j.jlp.2019.103983.
Elghobashi, S., 1994. On predicting particle-laden turbulent flows. Appl. Sci. Res. 52, 309–329. https://doi.org/10.1007/BF00936835.
Gao, W., Zhong, S., Miao, N., Liu, H., 2013. Effect of ignition on the explosion behavior of 1-Octadecanol/air mixtures. Powder Technol. 241, 105–114. https://doi.org/10.1016/j.powtec.2013.03.015.
Going, J.E., Chatrathi, K., Cashdollar, K.L., 2000. Flammability limit measurements for dusts in 20-L and 1-m3 vessels. J. Loss Prev. Process. Ind. 13, 209–219. https://doi.org/10.1016/S0950-4230(99)00043-1.
ISO 6184-1:1985, 1985. Explosion Protection Systems, Part 1, Determination of Explosion Indices of Combustible Dusts in Air Hauert, F., Vogl, A., 1995. Measurement of Dust Cloud Characteristics in Industrial Plants (Number: PL 910695).
Kalejaiye, O., 2001. An Investigation of the Effectiveness of Dust Dispersion in the Siwek 20-l Chamber. Dalhousie University, Halifax, Nova Scotia.
Kalejaiye, O., Amyotte, P.R., Pegg, M.J., Cashdollar, K.L., 2010. Effectiveness of dust dispersion in the 20-L Siwek chamber. J. Loss Prev. Process. Ind. 23, 46–59. https://doi.org/10.1016/j.jlp.2009.05.008.
Marmo, L., Cavallero, D., 2008. Minimum ignition energy of nylon fibres. J. Loss Prev. Process. Ind. 21, 512–517. https://doi.org/10.1016/j.jlp.2008.04.003.
Mercer, D.B., Amyotte, P.R., Dupuis, D.J., Pegg, M.J., Dahoe, A., De Heij, W.B.C., Zevenbergen, J.F., Scarlett, B., 2001. The influence of injector design on the decay of pre-ignition turbulence in a spherical explosion chamber. J. Loss Prev. Process. Ind. 14, 269–282. https://doi.org/10.1016/S0950-4230(00)00051-6.
Mintz, K.J., 1995. Problems in experimental measurements of dust explosions. J. Hazard Mater. 42, 177–186. https://doi.org/10.1016/0304-3894(95)00011-I.
Portarapillo, M., Di Sarli, V., Sanchirico, R., Di Benedetto, A., 2020a. CFD simulation of the dispersion of binary dust mixtures in the 20 L vessel. J. Loss Prev. Process. Ind. 67, 104231 https://doi.org/10.1016/j.jlp.2020.104231.
Portarapillo, M., Trofa, M., Sanchirico, R., Di Benedetto, A., 2020b. CFD simulations of dust dispersion in the 1 m3 explosion vessel. J. Loss Prev. Process. Ind. 68, 104274 https://doi.org/10.1016/j.jlp.2020.104274.
Portarapillo, M., Sanchirico, R., Di Benedetto, A., 2021a. On the pyrotechnic ignitors role in dust explosion testing : comparison between 20 L and 1 m 3 explosion vessels. Process Saf. Prog. 1–7 https://doi.org/10.1002/prs.12249.
Portarapillo, M., Sanchirico, R., Di Benedetto, A., 2021b. Effect of turbulence spatial distribution on the deflagration index: comparison between 20 L and 1 m3 vessels. J. Loss Prev. Process. Ind. 71 https://doi.org/10.1016/j.jlp.2021.104484.
Portarapillo, M., Trofa, M., Sanchirico, R., Di Benedetto, A., 2021c. CFD simulations of the effect of dust diameter on the dispersion in the 1 m3 explosion vessel. Chem. Eng. Trans. 86.
Portarapillo, Maria, Danzi, E., Guida, G., Luciani, G., Marmo, L., Sanchirico, R., Di Benedetto, A., 2022a. On the flammable behavior of non-traditional dusts: dimensionless numbers evaluation for nylon 6,6 short fibers. J. Loss Prev. Process. Ind. 78, 104815 https://doi.org/10.1016/j.jlp.2022.104815.
Portarapillo, M., Trofa, M., Sanchirico, R., Di Benedetto, A., 2022b. CFD simulation of turbulent fluid flow and dust dispersion in the 1 m3 explosion Vessel equipped with the rebound nozzle. J. Loss Prev. Process. Ind. 76, 104755 https://doi.org/10.1016/j.jlp.2022.104755.
Pu, Y.K., Jarosinski, J., Johnson, V.G., Kauffman, C.W., 1990. Turbulence effects on dust explosions in the 20-liter spherical vessel. Symp. Combust. 23, 843–849. https://doi.org/10.1016/S0082-0784(06)80338-3.
Rodgers, S.A., Ural, E.A., 2011. Practical issues with marginally explosible dusts—evaluating the real hazard. Process Saf. Prog. 30, 266–279. https://doi.org/10.1002/prs.
Shag, Y., You, F., 2013. The effect of particle size on the minimum ignition temperature of flour powder. 1st CCPS Asia-Pacific Conf. Process Saf 2013, 586–593, 2013.
Taveau, J.R., Going, J.E., Hochgreb, S., Lemkowitz, S.M., Roekaerts, D.J.E.M., 2017. Igniter-induced hybrids in the 20-l sphere. J. Loss Prev. Process. Ind. 49, 348–356. https://doi.org/10.1016/j.jlp.2017.07.014.
van der Wel, P.G.J., van Veen, J.P.W., Lemkowitz, S.M., Scarlett, B., van Wingerden, C.J. M., 1992. An interpretation of dust explosion phenomena on the basis of time scales. Powder Technol. 71, 207–215. https://doi.org/10.1016/0032-5910(92)80010-T.
Zhen, G., Leuckel, W., 1996. Determination of dust-dispersion-lnduced turbulence and its influence on dust explosions. Combust. Sci. Technol. 113, 629–639. https://doi.org/10.1080/00102209608935518.